MIT Libraries | DSpace@MIT

MIT Open Access Articles

COMPLETE ELEMENT ABUNDANCES OF NINE STARS IN THE r-PROCESS GALAXY RETICULUM II

Massachusetts Institute of Technology

COMPLETE ELEMENT ABUNDANCES OF NINE STARS IN THE *r*-PROCESS GALAXY RETICULUM II[*]

ALEXANDER P. JI[1,2], ANNA FREBEL[1,2], JOSHUA D. SIMON[3], AND ANIRUDH CHITI[1]
[1] Department of Physics and Kavli Institute for Astrophysics and Space Research, Massachusetts Institute of Technology,
Cambridge, MA 02139, USA; alexji@mit.edu
[2] Joint Institute for Nuclear Astrophysics—Center for Evolution of the Elements, East Lansing, MI:48824, USA
[3] Observatories of the Carnegie Institution of Washington, 813 Santa Barbara St., Pasadena, CA 91101, USA

ABSTRACT

We present chemical abundances derived from high-resolution *Magellan*/Magellan Inamori Kyocera Echelle spectra of the nine brightest known red giant members of the ultra-faint dwarf galaxy Reticulum II (Ret II). These stars span the full metallicity range of Ret II ($-3.5 < $ [Fe/H] $ < -2$). Seven of the nine stars have extremely high levels of *r*-process material ([Eu/Fe] ~ 1.7), in contrast to the extremely low neutron-capture element abundances found in every other ultra-faint dwarf galaxy studied to date. The other two stars are the most metal-poor stars in the system ([Fe/H] < -3), and they have neutron-capture element abundance limits similar to those in other ultra-faint dwarf galaxies. We confirm that the relative abundances of Sr, Y, and Zr in these stars are similar to those found in *r*-process halo stars, but they are ~ 0.5 dex lower than the solar *r*-process pattern. If the universal *r*-process pattern extends to those elements, the stars in Ret II display the least contaminated known *r*-process pattern. The abundances of lighter elements up to the iron peak are otherwise similar to abundances of stars in the halo and in other ultra-faint dwarf galaxies. However, the scatter in abundance ratios is large enough to suggest that inhomogeneous metal mixing is required to explain the chemical evolution of this galaxy. The presence of low amounts of neutron-capture elements in other ultra-faint dwarf galaxies may imply the existence of additional *r*-process sites besides the source of *r*-process elements in Ret II. Galaxies like Ret II may be the original birth sites of *r*-process enhanced stars now found in the halo.

Key words: galaxies: dwarf – galaxies: individual (Ret II) – Local Group – nuclear reactions, nucleosynthesis, abundances – stars: abundances

Supporting material: machine-readable table

1. INTRODUCTION

Ultra-faint dwarf galaxies (UFDs) probe extreme astrophysical regimes. They are the faintest and most metal-poor galaxies known (Kirby et al. 2008, 2013). Their high velocity dispersions imply that they are the most dark-matter-dominated galaxies (Simon & Geha 2007; Strigari et al. 2008; Simon et al. 2011), making them attractive targets for indirect dark matter searches (e.g., Drlica-Wagner et al. 2015). The bulk of their star formation occurs before reionization (Brown et al. 2014), and they may be important sources of ionizing photons (Weisz et al. 2014; Wise et al. 2014). The initial mass function in UFDs differs from more massive galaxies (Geha et al. 2013). Most importantly for our current purpose, UFDs provide a coherent environment in which to probe the earliest stages of nucleosynthesis and chemical evolution (Frebel & Bromm 2012; Karlsson et al. 2013; Ji et al. 2015). Reticulum II (Ret II) is a UFD recently discovered in the Dark Energy Survey (Koposov et al. 2015a; Bechtol et al. 2015). Its velocity dispersion and metallicity spread confirm it to be a galaxy, and it is one of the most metal-poor galaxies known (Koposov et al. 2015b; Simon et al. 2015; Walker et al. 2015). At only ~30 kpc away, it contains stars within the reach of high-resolution spectroscopy for abundance analysis.

Until recently, nearly all UFD stars observed with high-resolution spectroscopy displayed unusually low neutron-capture element abundances compared to halo star abundances ([X/Fe] $\lesssim -1$) (e.g., Frebel et al. 2010, 2014; Koch

et al. 2013). However, Ji et al. (2016a) and Roederer et al. (2016b) reported that seven of the nine stars they observed in Ret II have highly enhanced neutron-capture abundances ([Eu/Fe] ~ 1.7). Moreover, the relative abundances of the elements heavier than barium match the scaled solar *r*-process pattern (Sneden et al. 2008), confirming that the universality of this nucleosynthesis process holds for stars in the faintest dwarf galaxies (also see Aoki et al. 2007b). Metal-poor stars with this level of *r*-process enhancement ([Eu/Fe] > 1, or *r*-II stars, Christlieb et al. 2004) are only rarely found in the halo (Barklem et al. 2005; Roederer et al. 2014a). The striking 2−3 orders of magnitude difference between the neutron-capture element content of Ret II and that of the other UFDs is clear evidence that a single rare and prolific *r*-process event is responsible for nearly all neutron-capture material in Ret II (Ji et al. 2016a). In addition to the usual questions about the formation history of UFDs and possible signatures of the first stars, this galaxy provides a tremendous opportunity to study the origin of the *r*-process elements.

Roederer et al. (2016b) presented the first high-resolution abundance measurements of elements lighter than barium in four Ret II stars. They found that the abundances of Sr, Y, and Zr in the three *r*-process-rich Ret II stars were similar to those of the *r*-II star CS22892−052. They also found that the abundances of the sub-iron-peak elements were generally consistent with halo star abundances at similar metallicities, implying that the source of *r*-process elements in Ret II either produced none of these elements or produced them in similar amounts to core-collapse supernovae. Roederer et al. (2016b) also found abundance variations for different stars with similar

Table 1
Observed Stars and Stellar Parameters

Star	t_{exp} (min)	V (mag)	S/N (4250 Å)	S/N (6000 Å)	v_{helio} (km s^{-1})	T_{eff} (K)	$\log g$ (dex)	ν_{micr} (km s^{-1})	[Fe/H]
DES J033523−540407	75	16.04	22	47	66.8 ± 0.1	4608 ± 157	1.00 ± 0.30	2.40 ± 0.29	−3.01
DES J033607−540235	110	17.11	12	27	62.7 ± 0.1	4833 ± 166	1.55 ± 0.34	2.15 ± 0.28	−2.97
DES J033447−540525	58	17.20	11	22	62.0 ± 0.1	4900 ± 170	1.70 ± 0.31	1.90 ± 0.28	−2.91
DES J033531−540148	165	17.34	16	32	60.9 ± 0.1	4925 ± 163	1.90 ± 0.36	1.80 ± 0.28	−3.34
DES J033548−540349	165	17.96	12	25	61.9 ± 0.1	5125 ± 162	2.35 ± 0.32	1.75 ± 0.28	−2.19
DES J033537−540401	165	18.28	10	19	63.5 ± 0.2	5170 ± 201	2.45 ± 0.37	1.55 ± 0.36	−2.73
DES J033556−540316	220	18.59	11	19	62.7 ± 0.2	5305 ± 258	2.95 ± 0.40	1.65 ± 0.40	−3.54
DES J033457−540531	110	18.66	8	16	61.9 ± 0.1	5328 ± 183	2.85 ± 0.32	1.50 ± 0.30	−2.08
DES J033454−540558	205	18.68	7	13	71.6 ± 0.3	5395 ± 249	3.10 ± 0.40	1.35 ± 0.42	−2.77

Note. All stars were observed with a 1″0 slit. Signal-to-noise is per pixel. *V* magnitudes were found with the conversion in Bechtol et al. (2015). Velocity error is from FWHM of cross-correlation. See Ji et al. (2016a) for stellar parameter uncertainty breakdown.

[Fe/H], which suggests that metals are not uniformly mixed into the galaxy's gas reservoir. Accounting for this inhomogeneous metal mixing is important when using chemical abundances to understand the formation of this galaxy (e.g., Webster et al. 2016).

Here, we report the complete chemical abundance patterns for the nine Reticulum II stars considered by Ji et al. (2016a), including the four investigated by Roederer et al. (2016b). Our stars span the entire metallicity range of Ret II (Simon et al. 2015). In Section 2 we describe the observations and abundance analysis. The abundance patterns are reported in Section 3. In Section 4 we discuss implications for nuclear astrophysics and the *r*-process site. In Section 5 we consider possibilities for using this galaxy to understand early star and galaxy formation. We conclude in Section 6.

2. OBSERVATIONS AND ABUNDANCE ANALYSIS

2.1. Observations

On 2015 October 1–4 we obtained high-resolution spectra of the brightest nine confirmed members in Ret II (Simon et al. 2015). We used the Magellan Inamori Kyocera Echelle (MIKE) spectrograph (Bernstein et al. 2003) on the *Magellan*-Clay telescope with a 1″0 slit, which provides a spectral resolution of ~22,000 and ~28,000 at red and blue wavelengths, respectively. We used 2 × 2 on-chip binning to reduce read noise. Individual exposure times were typically 55 minutes to minimize cosmic rays, except for DES J033523−540407, which was observed with 20–30 minute exposures. Stars were observed for 1–4 hr each, resulting in signal-to-noise of 13–47 at 6000 Å and 7–22 at 4250 Å. Table 1 contains more observation details. Thin to moderate clouds were sometimes present, resulting in the different exposure times required to achieve comparable signal-to-noise for stars of similar magnitudes (e.g., DES J033457−540531 and DES J033454−540558).

We used the CarPy MIKE pipeline to reduce all exposures to a single spectrum (Kelson 2003).[4] Using the SMH analysis software from Casey (2014), we normalized and stitched echelle orders together before Doppler correcting the spectra by cross-correlation with a spectrum of HD122563 using the Mg triplet lines near 5200 Å. Heliocentric velocities were determined with `rvcor` in IRAF. Figure 1 shows selected spectral

regions. The regions around the 4129 Å Eu line and the 4554 Å Ba line are shown in Ji et al. (2016a).

2.2. Chemical Abundance Analysis

The overall abundance analysis method is described in Frebel et al. (2013) and Ji et al. (2016a), which we review for completeness. We measured equivalent widths, determined stellar parameters, and derived chemical abundances using SMH (Casey 2014). The Castelli & Kurucz (2004) model atmospheres with *α*-enhancement were used with the one-dimensional (1D) plane-parallel LTE abundance analysis code MOOG (Sneden 1973). We use a MOOG version that accounts for Rayleigh scattering (Sobeck et al. 2011). Abundances are normalized to the solar abundances in Asplund et al. (2009).
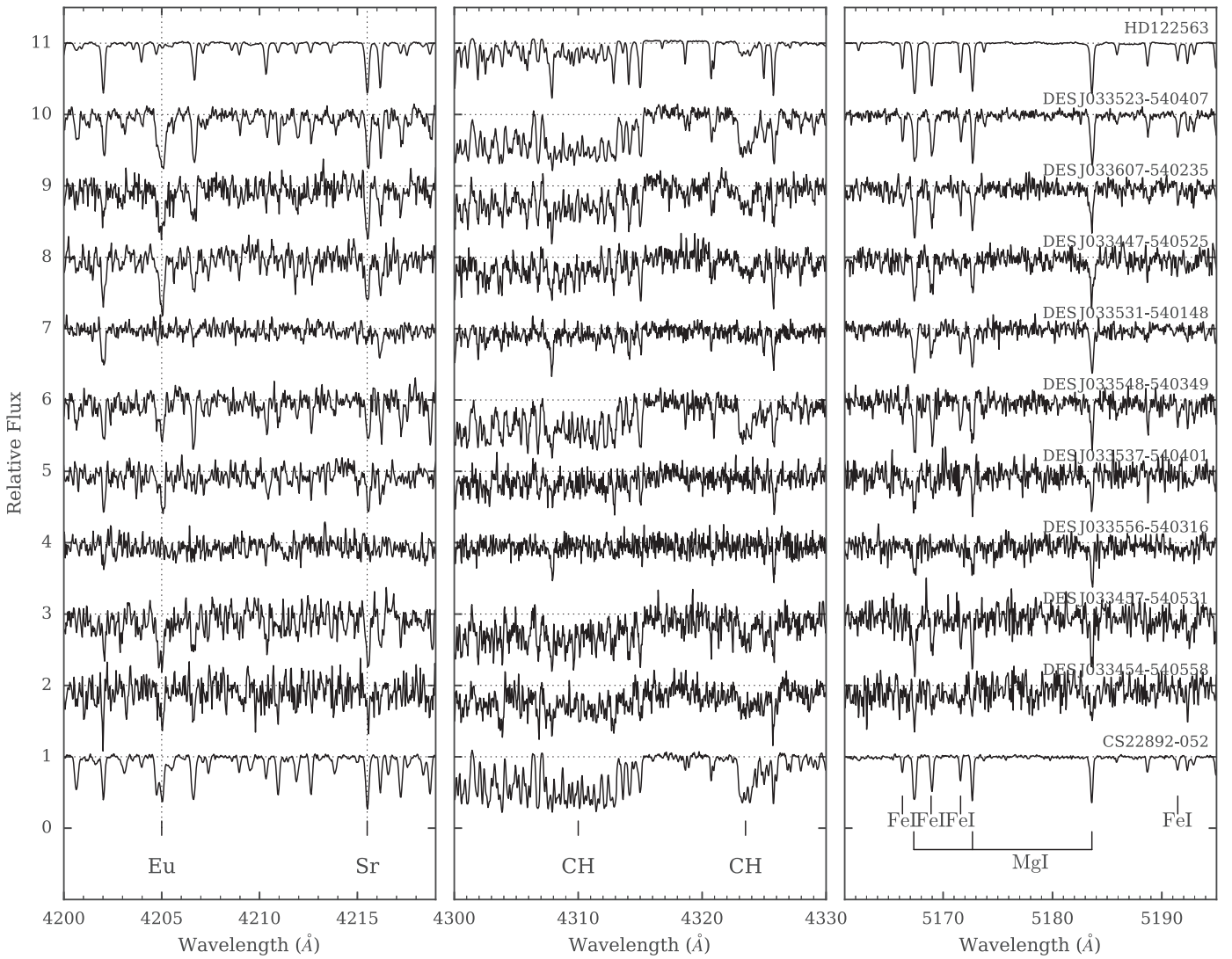
With SMH, we measure equivalent widths by fitting Gaussian profiles to the line list from Roederer et al. (2010b). We exclude lines with reduced equivalent widths larger than −4.5 unless they were the only lines available, since such lines are likely past the linear regime of the curve of growth. In particular, we often retained the 4226 Å Ca line, the 5172 Å Mg line, and the 5183 Å Mg line despite their large reduced equivalent widths. Atomic data for neutron-capture lines were compiled from several sources (primarily Hill et al. 2002; Ivans et al. 2006; supplemented with Den Hartog et al. 2003; Lawler et al. 2006, 2009; Sneden et al. 2009 where appropriate). Carbon was synthesized with the line list from Masseron et al. (2014).[5]

We estimate equivalent width uncertainties with the formula from Frebel et al. (2006) (originally Bohlin et al. 1983). For most stars the percent uncertainty is 10%–20%. The brightest star, DES J033523−540407, has 5%–10% uncertainty, while the fainter stars DES J033556−540316, DES J033457−540531, and DES J033454−540558 have 15%–30% uncertainty, largely due to their lower signal-to-noise. Table 2 contains our equivalent width measurements. The abundances of blended lines, molecular bands, and lines with hyperfine structure were determined with spectrum synthesis. The abundances of C, Sc, Mn, Sr, Ba, La, and Eu are determined only through synthesis. Some lines of Al, Si, Y, Pr, and Dy are also synthesized. For Ba and Eu, we adopt the *r*-process-only isotope ratios (Sneden et al. 2008).

We followed the procedure described by Frebel et al. (2013) to derive stellar parameters, including the effective temperature correction. For DES J033556−540316 and DES J033454

---

[4] http://code.obs.carnegiescience.edu/mike　　　　　　　　[5] Adapted from http://kurucz.harvard.edu/molecules/ch/.

Figure 1. Spectra of nine stars in Ret II around neutron-capture lines, the carbon G-band, and the magnesium triplet. Stars are ordered by brightness (as in Table 1). For comparison, we show spectra for the star HD122563 and the *r*-II star CS22892−052.

Table 2
Equivalent Widths

El.	λ (Å)	χ (eV)	log *gf* (dex)	EW (mÅ)	log $\epsilon(X)$ (dex)
					DES J033523−540407
CH	4313	⋯	⋯	syn	6.07
CH	4323	⋯	⋯	syn	6.07
Na I	5889.95	0.00	0.11	178.6	3.59
Na I	5895.92	0.00	−0.19	151.9	3.47

(This table is available in its entirety in machine-readable form.)

−540558, no Fe II lines were measurable so we determined their log *g* from an isochrone (Kim et al. 2002). We determined statistical errors in the stellar parameters by varying them to match the 1σ errors in the relevant slopes (see Ji et al. 2016a). We additionally adopted systematic stellar parameter uncertainties of 150K for $T_{\rm eff}$, 0.3 dex for log *g*, and 0.2 km s^{-1} for $\nu_{\rm micr}$, which were added in quadrature to the statistical uncertainties. Table 1 contains the final stellar parameters and uncertainties.

Table 3 shows the abundances of the nine stars in Reticulum II. The uncertainty σ denotes the standard deviation of the abundance measured for individual lines. If fewer than 10 lines are measured for an element, the standard deviation is instead calculated with an unbiased estimator accounting for the small number of lines (Keeping 1962). If only a single line is available, the uncertainty is estimated by extreme continuum placements. For elements with an abundance that is determined with synthesis, the uncertainty reflects the 1σ noise in the synthesized fit. The standard deviation for some elements is unreasonably small, and we consider the standard deviation of the Fe I lines as the minimum standard deviation for any element in a given star.

Table 4 shows the abundance uncertainties due to stellar parameter uncertainties for DES J033523−540407. Changing the model atmosphere metallicity by 0.2 dex results in <0.02 dex additional error in the abundances. As our nine stars are all red giants, scaling these abundance errors linearly with the uncertainty in stellar parameters is a reasonable approximation for the other stars (Roederer et al. 2014b).

3

Table 3
Chemical Abundances

Species	N	$\log \epsilon(X)$	σ	[X/H]	[X/Fe]	N	$\log \epsilon(X)$	σ	[X/H]	[X/Fe]	N	$\log \epsilon(X)$	σ	[X/H]	[X/Fe]
		DES J033523−540407					DES J033607−540235					DES J033447−540525			
C	2	6.07	0.15	−2.36	0.65	2	5.86	0.20	−2.57	0.40	2	5.72	0.22	−2.71	0.20
Na I	2	3.53	0.11	−2.71	0.30	2	3.42	0.16	−2.82	0.15	2	3.68	0.21	−2.56	0.35
Mg I	4	5.05	0.25	−2.55	0.46	3	5.01	0.09	−2.59	0.38	4	5.14	0.32	−2.46	0.44
Al I	2	2.78	0.27	−3.67	−0.66	1	2.74	0.30	−3.71	−0.74	1	2.79	0.38	−3.66	−0.75
Si I	1	5.19	0.28	−2.32	0.69	1	4.99	0.50	−2.52	0.45	1	4.86	0.32	−2.65	0.26
Ca I	9	3.53	0.09	−2.81	0.20	9	3.74	0.21	−2.60	0.37	4	3.75	0.21	−2.59	0.31
Sc II	5	−0.03	0.13	−3.18	−0.17	5	0.32	0.15	−2.83	0.14	5	0.16	0.16	−2.99	−0.09
Ti I	7	2.10	0.18	−2.85	0.16	⋯	⋯	⋯	⋯	⋯	⋯	⋯	⋯	⋯	⋯
Ti II	27	2.23	0.20	−2.72	0.29	16	2.34	0.19	−2.61	0.36	15	2.21	0.18	−2.74	0.17
Cr I	5	2.22	0.27	−3.42	−0.41	5	2.44	0.21	−3.20	−0.24	3	2.54	0.54	−3.10	−0.20
Mn I	5	2.04	0.13	−3.39	−0.38	3	1.59	0.12	−3.84	−0.87	3	1.52	0.24	−3.91	−1.00
Fe I	128	4.49	0.16	−3.01	0.00	103	4.53	0.21	−2.97	0.00	104	4.59	0.19	−2.91	0.00
Fe II	5	4.43	0.09	−3.07	−0.06	8	4.64	0.12	−2.86	0.11	10	4.60	0.13	−2.90	0.00
Co I	6	2.04	0.32	−2.95	0.06	4	2.34	0.30	−2.65	0.32	5	2.45	0.15	−2.54	0.37
Ni I	4	3.04	0.29	−3.17	−0.16	3	3.10	0.22	−3.12	−0.15	2	3.31	0.23	−2.91	0.00
Sr II	2	0.03	0.30	−2.83	0.18	2	0.53	0.40	−2.35	0.62	2	0.32	0.50	−2.56	0.35
Y II	9	−0.48	0.24	−2.69	0.32	5	−0.12	0.18	−2.33	0.64	3	−0.21	0.12	−2.42	0.49
Zr II	3	0.08	0.06	−2.50	0.51	6	0.46	0.15	−2.12	0.85	4	0.59	0.16	−1.99	0.92
Ba II	5	−0.04	0.21	−2.22	0.79	5	0.12	0.17	−2.06	0.91	5	0.35	0.30	−1.83	1.08
La II	3	−0.81	0.18	−1.91	1.10	3	−0.64	0.20	−1.74	1.23	2	−0.51	0.50	−1.61	1.30
Ce II	6	−0.51	0.13	−2.09	0.92	2	−0.15	0.10	−1.74	1.23	3	−0.02	0.24	−1.60	1.31
Pr II	1	−1.09	0.20	−1.81	1.20	2	−0.67	0.33	−1.39	1.58	1	−0.79	0.40	−1.51	1.40
Nd II	14	−0.21	0.29	−1.63	1.38	11	−0.01	0.20	−1.43	1.54	8	0.25	0.22	−1.17	1.74
Sm II	3	−0.65	0.09	−1.61	1.40	3	−0.28	0.11	−1.24	1.73	2	−0.06	0.31	−1.01	1.89
Eu II	5	−0.81	0.15	−1.33	1.68	4	−0.71	0.22	−1.23	1.74	3	−0.52	0.20	−1.04	1.86
Gd II	3	−0.47	0.27	−1.54	1.47	1	−0.14	0.31	−1.21	1.76	⋯	⋯	⋯	⋯	⋯
Dy II	5	−0.29	0.31	−1.39	1.62	3	−0.15	0.46	−1.25	1.72	5	0.20	0.24	−0.90	2.01
		DES J033531−540148					DES J033548−540349					DES J033537−540401			
C	2	5.29	0.30	−3.14	0.20	2	6.74	0.18	−1.69	0.50	2	5.85	0.34	−2.58	0.15
Na I	2	3.87	0.02	−2.37	0.97	2	3.96	0.01	−2.28	−0.08	2	3.65	0.44	−2.59	0.14
Mg I	5	4.95	0.12	−2.65	0.69	3	5.33	0.25	−2.27	−0.08	4	5.05	0.37	−2.55	0.18
Al I	2	2.44	0.49	−4.02	−0.68	1	< 3.66	⋯	< −2.79	<−0.60	1	<3.60	⋯	<−2.85	<−0.12
Si I	2	4.71	0.60	−2.80	0.54	1	5.34	0.24	−2.17	0.02	1	5.08	0.60	−2.43	0.30
Ca I	6	3.32	0.22	−3.02	0.31	14	4.54	0.23	−1.80	0.40	4	3.80	0.24	−2.54	0.19
Sc II	5	0.11	0.13	−3.04	0.30	4	0.28	0.19	−2.87	−0.67	4	0.42	0.24	−2.73	0.00
Ti I		⋯	⋯	⋯	⋯	10	3.16	0.15	−1.79	0.40		⋯	⋯	⋯	⋯
Ti II	15	2.04	0.18	−2.91	0.42	36	3.39	0.19	−1.56	0.64	12	2.51	0.30	−2.44	0.29
Cr I	3	2.07	0.05	−3.57	−0.23	10	3.47	0.10	−2.17	0.03	2	2.51	0.07	−3.13	−0.40
Mn I	3	1.34	0.27	−4.09	−0.75	6	2.84	0.31	−2.59	−0.40	1	<3.70	⋯	<−1.73	<1.00
Fe I	80	4.16	0.14	−3.34	0.00	124	5.31	0.19	−2.19	0.00	51	4.77	0.21	−2.73	0.00
Fe II	3	4.15	0.19	−3.35	−0.01	12	5.32	0.10	−2.18	0.02	3	4.76	0.17	−2.74	−0.01
Co I	1	2.39	0.35	−2.60	0.74	2	3.01	0.25	−1.98	0.21	1	<3.51	⋯	<−1.48	<1.25
Ni I	2	2.71	0.23	−3.51	−0.17	2	4.10	0.64	−2.12	0.07	1	<4.86	⋯	<−1.36	<1.37
Zn I		⋯	⋯	⋯	⋯	2	3.29	0.27	−1.27	0.92		⋯	⋯	⋯	⋯
Sr II	1	<−1.37	⋯	<−4.24	<−0.90	2	0.33	0.32	−2.54	−0.35	2	0.36	0.50	−2.50	0.23
Y II		⋯	⋯	⋯	⋯	2	−0.09	0.10	−2.29	−0.10	2	0.41	0.13	−1.80	0.93
Ba II	1	<−1.96	⋯	<−4.14	<−0.80	5	0.35	0.30	−1.83	0.36	5	0.85	0.30	−1.33	1.40
Nd II		⋯	⋯	⋯	⋯	4	0.35	0.23	−1.07	1.13		⋯	⋯	⋯	⋯
Eu II	1	<−1.32	⋯	<−1.84	<1.50	2	−0.72	0.27	−1.24	0.95	2	−0.51	0.36	−1.03	1.70
Dy II		⋯	⋯	⋯	⋯	2	0.15	0.47	−0.95	1.25	2	0.16	0.78	−0.94	1.79
		DES J033556−540316					DES J033457−540531					DES J033454−540558			
C	1	<6.09	⋯	<−2.34	<1.20	2	6.70	0.35	−1.73	0.35	2	6.51	0.25	−1.92	0.85
Na I	2	3.18	0.05	−3.06	0.48	2	4.25	0.38	−1.99	0.09	2	3.37	0.29	−2.88	−0.11
Mg I	2	4.60	0.33	−3.00	0.53	6	5.76	0.24	−1.84	0.24	2	5.00	0.13	−2.59	0.17
Al I	1	<2.71	⋯	<−3.74	<−0.20	2	3.38	0.27	−3.07	−0.99	1	<3.76	⋯	<−2.69	<0.08
Si I	1	<5.49	⋯	<−2.02	<1.52	2	5.98	0.50	−1.53	0.55	1	<7.27	⋯	<−0.24	<2.53
Ca I	3	3.23	0.33	−3.11	0.42	5	4.58	0.17	−1.76	0.32	3	3.99	0.07	−2.35	0.42
Sc II	1	−0.29	0.70	−3.44	0.10	5	1.37	0.21	−1.78	0.30	1	0.54	0.50	−2.61	0.16
Ti II	6	2.03	0.29	−2.92	0.62	14	3.35	0.21	−1.60	0.48	9	2.63	0.28	−2.32	0.45
Cr I	2	1.58	0.27	−4.05	−0.52	3	3.37	0.12	−2.27	−0.20	1	2.37	0.00	−3.27	−0.50

Table 3
(Continued)

Species	N	log ε(X)	σ	[X/H]	[X/Fe]	N	log ε(X)	σ	[X/H]	[X/Fe]	N	log ε(X)	σ	[X/H]	[X/Fe]
Mn I	1	<2.69	⋯	<−2.74	<0.80	2	2.65	0.35	−2.78	−0.70	1	<4.17	⋯	<−1.26	<1.51
Fe I	33	3.96	0.18	−3.54	0.00	67	5.42	0.19	−2.08	0.00	31	4.73	0.22	−2.77	−0.00
Fe II	⋯	⋯	⋯	⋯	⋯	7	5.44	0.10	−2.06	0.01		⋯	⋯	⋯	⋯
Co I	1	<2.60	⋯	<−2.39	<1.15	1	<4.24	⋯	<−0.75	<1.33	1	<3.84	⋯	<−1.15	<1.62
Ni I	1	<4.76	⋯	<−1.46	<2.08	1	<4.46	⋯	<−1.76	<0.32	1	<5.01	⋯	<−1.21	<1.56
Sr II	1	<−0.67	⋯	<−3.54	<−0.00	2	1.17	0.41	−1.71	0.37	1	0.40	0.50	−2.47	0.30
Y II	⋯	⋯	⋯	⋯	⋯	2	0.98	0.18	−1.23	0.85		⋯	⋯	⋯	⋯
Ba II	1	<−1.26	⋯	<−3.44	<0.10	5	1.46	0.31	−0.72	1.36	4	0.81	0.42	−1.37	1.40
Ce II	⋯	⋯	⋯	⋯	⋯	1	0.75	0.37	−0.83	1.25		⋯	⋯	⋯	⋯
Nd II	⋯	⋯	⋯	⋯	⋯	3	1.18	0.80	−0.24	1.83		⋯	⋯	⋯	⋯
Eu II	1	<−0.62	⋯	<−1.14	<2.40	3	0.21	0.35	−0.31	1.76	2	−0.14	0.38	−0.66	2.11
Dy II	⋯	⋯	⋯	⋯	⋯	2	1.22	0.14	0.12	2.20		⋯	⋯	⋯	⋯

Table 4
Systematic Errors for DES J033523−540407

Element	$\Delta T_{\rm eff}$	$\Delta \log g$	$\Delta \nu_{\rm micr}$	Total
CH (syn)	+0.32	−0.27	−0.04	0.42
Na I	+0.19	−0.08	−0.17	0.27
Mg I	+0.13	−0.03	−0.03	0.14
Al I	+0.19	−0.10	−0.18	0.28
Si I	+0.18	−0.02	−0.08	0.20
Ca I	+0.13	−0.02	−0.03	0.13
Sc II (syn)	+0.07	+0.02	−0.05	0.09
Ti I	+0.23	−0.03	−0.04	0.24
Ti II	+0.04	+0.05	−0.07	0.09
Cr I	+0.21	−0.03	−0.09	0.23
Mn I (syn)	+0.20	−0.01	−0.06	0.21
Fe I	+0.21	−0.03	−0.07	0.22
Fe II	−0.02	+0.06	−0.08	0.10
Co I	+0.25	−0.02	−0.06	0.26
Ni I	+0.24	−0.04	−0.17	0.30
Sr II (syn)	+0.23	+0.09	−0.21	0.32
Y II	+0.09	+0.05	−0.10	0.14
Zr II	+0.08	+0.06	−0.04	0.11
Ba II (syn)	+0.14	+0.05	−0.14	0.20
La II (syn)	+0.09	+0.09	−0.01	0.13
Ce II	+0.10	+0.07	−0.02	0.12
Pr II (syn)	+0.14	+0.09	+0.03	0.17
Nd II	+0.11	+0.05	−0.06	0.13
Sm II	+0.10	+0.06	−0.03	0.12
Eu II (syn)	+0.11	+0.10	+0.03	0.15
Gd II	+0.10	+0.06	−0.03	0.12
Dy II	+0.10	+0.05	−0.07	0.13

3. RETICULUM II ABUNDANCE SIGNATURE

We now discuss the chemical abundances of individual elements in Ret II and compare the abundance signature of the Ret II stars to stars in the stellar halo and in other UFDs. Figure 2 shows the light elements, and Figure 3 shows the neutron-capture elements. The halo stars are combined from the literature compilation in Frebel (2010); (including *r*-II stars from Westin et al. 2000; Hill et al. 2002; Sneden et al. 2003; Christlieb et al. 2004; Honda et al. 2004; Barklem et al. 2005; Preston et al. 2006; Frebel et al. 2007; Lai et al. 2008; Hayek et al. 2009). We have added the *r*-II stars from Aoki et al. (2010) and Li et al. (2015). This sample also includes some stars in dwarf spheroidals (dSphs), including an *r*-II star found in the Ursa Minor dSph (Aoki et al. 2007b). To this sample, we have added the stars from Roederer et al. (2014b). When stars

in these samples are duplicated, we take the values from Frebel (2010).

Abundances of UFD stars are compiled from several sources: Boötes I (Norris et al. 2010a, 2010b; Gilmore et al. 2013; Ishigaki et al. 2014; Frebel et al. 2016), Boötes II (Ji et al. 2016b), Canes Venatici II (François et al. 2016), Coma Berenices (Frebel et al. 2010), Hercules (Koch et al. 2008, 2013; François et al. 2016), Leo IV (Simon et al. 2010; François et al. 2016), Segue 1 (Frebel et al. 2014), Segue 2 (Roederer & Kirby 2014), and Ursa Major (Frebel et al. 2010). We do not consider the more luminous dwarf galaxy CVn I a UFD, as there is a 2 magnitude gap between it and the next brightest satellite, Hercules (McConnachie 2012).

3.1. Carbon

Carbon abundances are determined by synthesizing two CH molecular absorption regions near 4313 Å and 4323 Å. Table 5 contains corrections for the stars' evolutionary statuses from (Placco et al. 2014). Note that the UFD stars (including Ret II) in Figure 2 have their carbon abundances corrected this way, but the halo star samples do not.

With the correction, we identify DES J033523−540407, DES J033607−540235, and DES J033454−540558 as carbon-enhanced metal-poor (CEMP) stars with [C/Fe] > 0.7 (Aoki et al. 2007a). In contrast to the expected CEMP fraction from halo stars (Placco et al. 2014), DES J033531−540148 has [Fe/H] = −3.34 but is not a CEMP star, even with the correction ([C/Fe]$_{\rm corrected}$ = 0.22). This appears to be the lowest [Fe/H] non-CEMP star in a UFD. One star in Boo I has an observed [C/Fe] = 0.25 (Norris et al. 2010b), but after the evolutionary status correction it has [C/Fe] = 0.90. DES J033556−540316 has an upper limit that does not exclude it from being a CEMP star. If this is not a CEMP star, then three out of nine stars in Ret II are CEMP stars, for a CEMP fraction of 33%. We discuss this more in Section 5.3.

Both the corrected and uncorrected carbon abundances vary significantly from star to star despite the similar *r*-process enhancements. Carbon is especially sensitive to the effective temperature, so the variation in the fainter stars could be attributed to stellar parameter uncertainties. However, as Roederer et al. (2016b) previously noted, even the three brightest stars have significantly different carbon abundances.
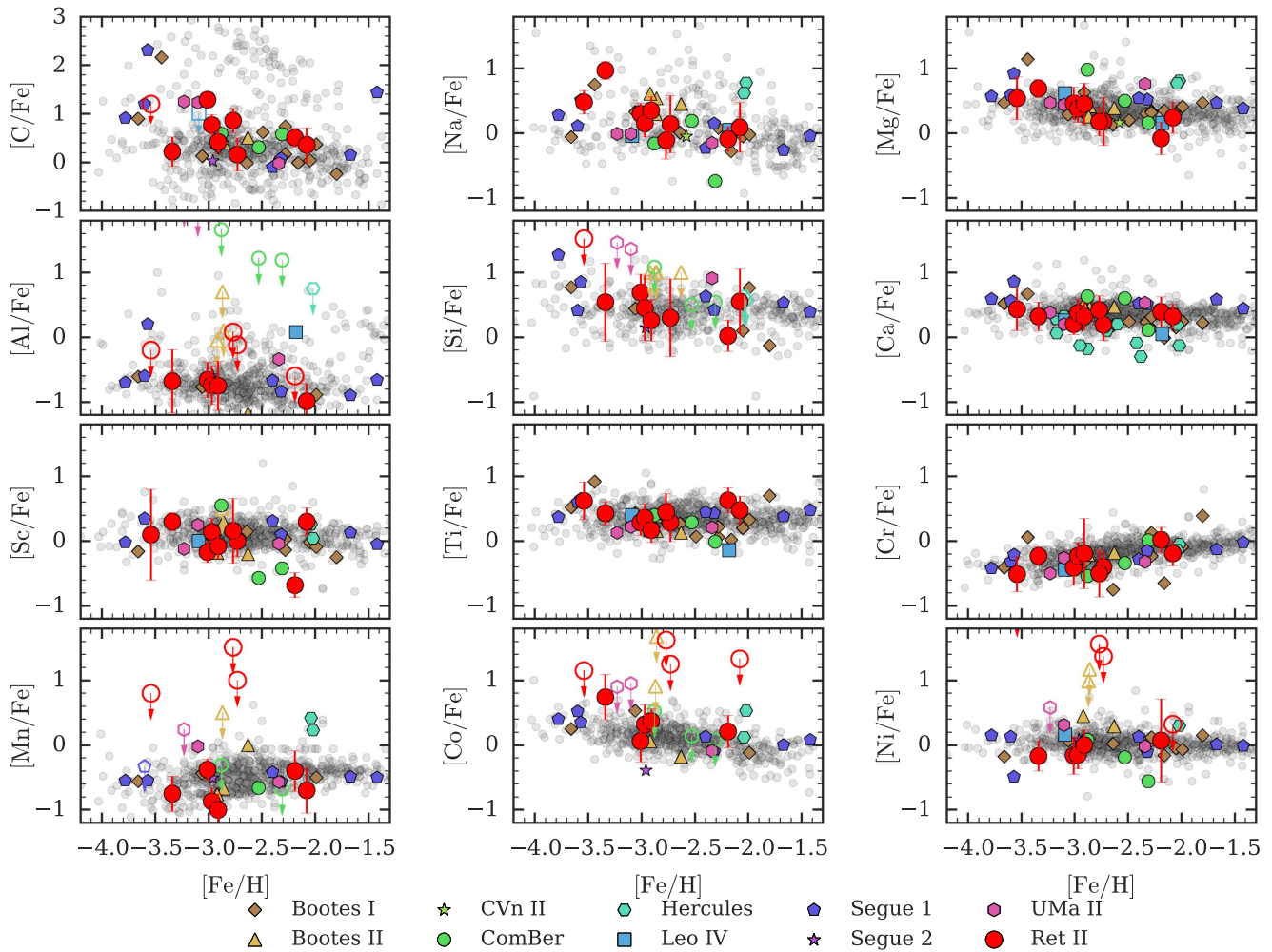
Figure 2. Abundances of light elements for Ret II (red points), UFD stars (colored points), and halo stars (gray points). See the text for references. Open symbols denote upper limits in UFDs. For clarity, we do not plot upper limits for the halo stars. Error bars indicate the standard deviation in Table 3, where the standard deviation of Fe II is taken as a minimum uncertainty. C abundances in UFDs are corrected for stellar evolutionary state (Table 5). Plotted Na abundances are uncorrected for LTE effects. The abundances of Ret II stars generally follow the abundance trends found in halo stars and other UFD stars. DES J033548−540349 has anomalously low Sc, and may also have low Mg and Si.

3.2. α-Elements: Mg, Si, Ca, Ti

Magnesium, calcium, and titanium abundances are derived from equivalent widths. We use the Ti II ion as the representative titanium abundance, as its stronger lines are detectable in all of our stars. Silicon abundances are derived from the 3905 Å and 4102 Å lines. The 3905 Å line is blended with carbon, and we avoid it when possible.

Stars whose iron content comes predominantly from core-collapse supernovae (instead of SNe Ia) typically have $[\alpha/\mathrm{Fe}] \sim 0.4$ (e.g., Tinsley 1979; Nomoto et al. 2013). Most of the α-abundances in our stars follow this trend, with the notable exception of DES J033548−540349. This star has low [Mg/Fe] and [Si/Fe] (∼0), but enhanced [Ca/Fe] and [Ti/Fe]. Since DES J033548−540349 has [Fe/H] = −2.19, a declining $[\alpha/\mathrm{Fe}]$ may be expected if SNe Ia have begun to contribute to the higher-metallicity stars (e.g., Kirby et al. 2011a). If so, it is strange that DES J033457−540531 (which also has [Fe/H] ∼ −2) appears to be α-enhanced, although there may be some variation in the abundance of different α-elements in this star. We discuss this more in Section 5.1. The two most metal-poor stars DES J033531−540148 and DES J033556−540316 appear to have somewhat enhanced [Mg/Fe], but the other α-

elements are normal. The variation between different α-elements in these stars demonstrates that a single average $[\alpha/\mathrm{Fe}]$ value may be insufficient to describe the abundances of these stars.

3.3. Iron-peak Elements: Cr, Mn, Co, Ni

Chromium, cobalt, and nickel abundances are derived from equivalent widths, while manganese abundances are derived from synthesis. We find no deviations of note from the overall halo pattern and other UFDs.

3.4. Odd-Z Elements: Na, Al, Sc

Sodium abundances are derived from the Na doublet. These lines have large NLTE corrections, which are determined with the models from Lind et al. (2011)[6] and given in Table 5. We plot the uncorrected abundances in Figure 2, as much of the halo sample does not have these corrections applied. DES J033531−540148 has an unusually high Na abundance, although it is still within the scatter of the halo stars.

---

[6] http://inspect-stars.com/
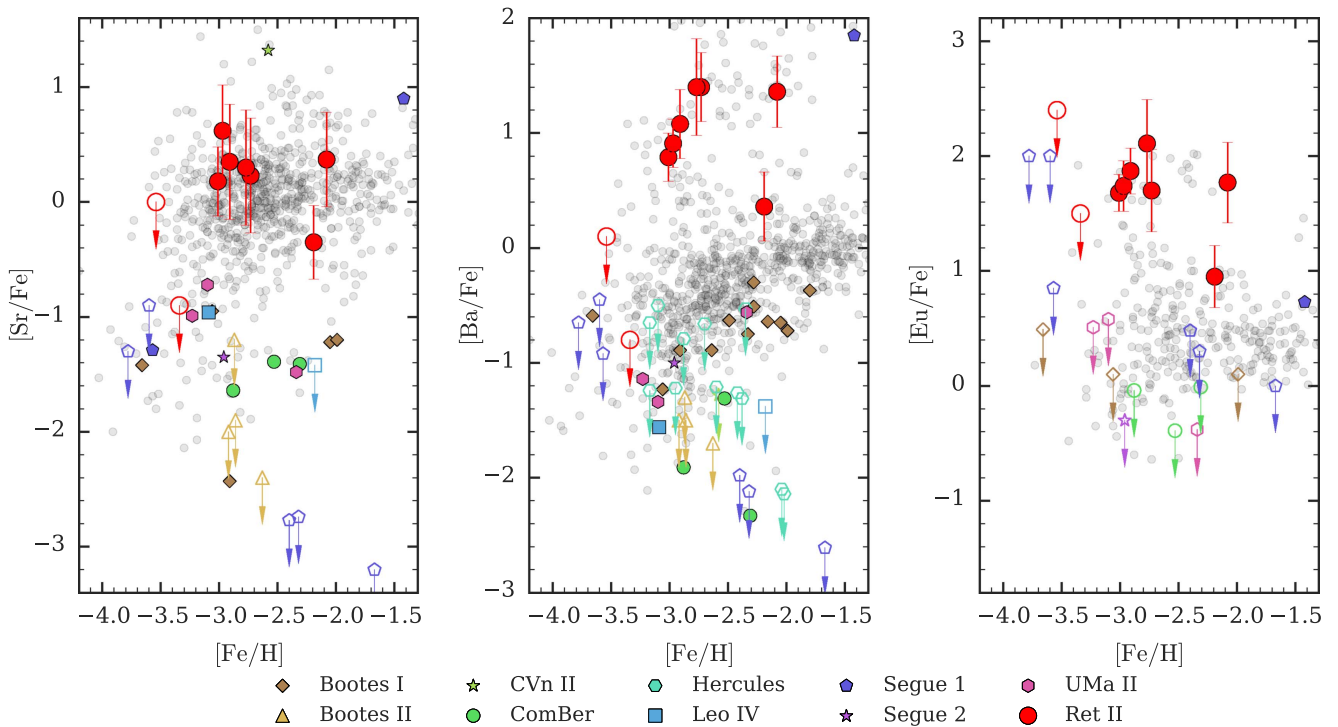
Figure 3. Neutron-capture element abundances for Sr, Ba, and Eu. Symbols are the same as in Figure 2. DES J033531−540148 and DES J033556−540316 have only upper limits that are consistent with other UFD stars. Note that DES J033531−540148 has a [Sr/Fe] = −1.73 detection (Roederer et al. 2016b). The other seven stars have extremely enhanced neutron-capture abundances, although DES J033548−540349 is less enhanced. CVn II has a star with very high [Sr/Fe] but no detectable Ba (François et al. 2016). The star in Segue 1 with high neutron-capture abundances has experienced binary mass transfer (Frebel et al. 2014).

Table 5
Abundance Corrections

Star	[X/Fe]$_{orig}$	Correction	[X/Fe]$_{corr}$
Carbon (Placco et al. 2014)			
DES J033523−540407	0.65	0.64	1.29
DES J033607−540235	0.40	0.37	0.77
DES J033447−540525	0.20	0.22	0.42
DES J033531−540148	0.20	0.02	0.22
DES J033548−540349	0.50	0.01	0.51
DES J033537−540401	0.15	0.01	0.16
DES J033457−540531	0.35	0.01	0.36
DES J033454−540558	0.85	0.01	0.86
Sodium (Lind et al. 2011)			
DES J033523−540407	0.30	−0.55	−0.25
DES J033607−540235	0.15	−0.48	−0.33
DES J033447−540525	0.35	−0.58	−0.23
DES J033531−540148	0.97	−0.50	0.47
DES J033548−540349	−0.08	−0.64	−0.72
DES J033537−540401	0.14	−0.54	−0.40
DES J033556−540316	0.48	−0.27	0.21
DES J033457−540531	0.09	−0.63	−0.54
DES J033454−540558	−0.11	−0.34	−0.45

Aluminum abundances are derived from the 3961 Å and 3944 Å lines. The 3944 Å line is synthesized due to a carbon blend. These relatively blue lines are not detectable in stars with lower signal-to-noise, and we use the 3961 Å line to set upper limits.

The scandium lines are synthesized, as they have hyperfine structure. DES J033548−540349 has an unusually low scandium abundance compared to halo stars, with [Sc/Fe] = −0.68. This star is relatively metal-rich, with [Fe/H] = −2.19, but it is reminiscent of two stars in Coma Berenices (Frebel et al. 2010) and three metal-poor scandium-deficient bulge stars (Casey & Schlaufman 2015). Casey & Schlaufman (2015) discuss the possible implications of the low Sc for chemical evolution, although the larger samples of Howes et al. (2015) did not identify additional scandium-poor stars in the bulge.

3.5. Neutron-capture Elements

Sr, Ba, La, and Eu have abundances all derived from synthesis because of hyperfine structure. The abundances of other neutron-capture elements are mostly determined with equivalent widths, although some lines of Y, Pr, and Dy are synthesized due to blends. We cannot detect Pb or actinides (Th, U) in our spectra.

Sr, Ba, and Eu are detected or constrained in all of our stars (Figure 3). The two most metal-poor stars have only nondetections of neutron-capture elements, while the other seven stars have enhanced neutron-capture elements. Six of these stars are considered r-II stars with [Eu/Fe] ∼ 1.7. The other star (DES J033548−540349, [Fe/H] = −2.19) has a lower [Eu/Fe] = 0.95. In these seven stars, all detected elements above Ba follow the universal r-process pattern (Ji et al. 2016a).

However, this pattern is not necessarily universal for lighter neutron-capture elements such as Sr, Y, and Zr (e.g.,Travaglio et al. 2004; Montes et al. 2007). To examine this in detail, we investigate how the relative abundances of these elements differ from the scaled solar r-process pattern. Rather than using Ba or Eu as representative elements, we scale the solar pattern to
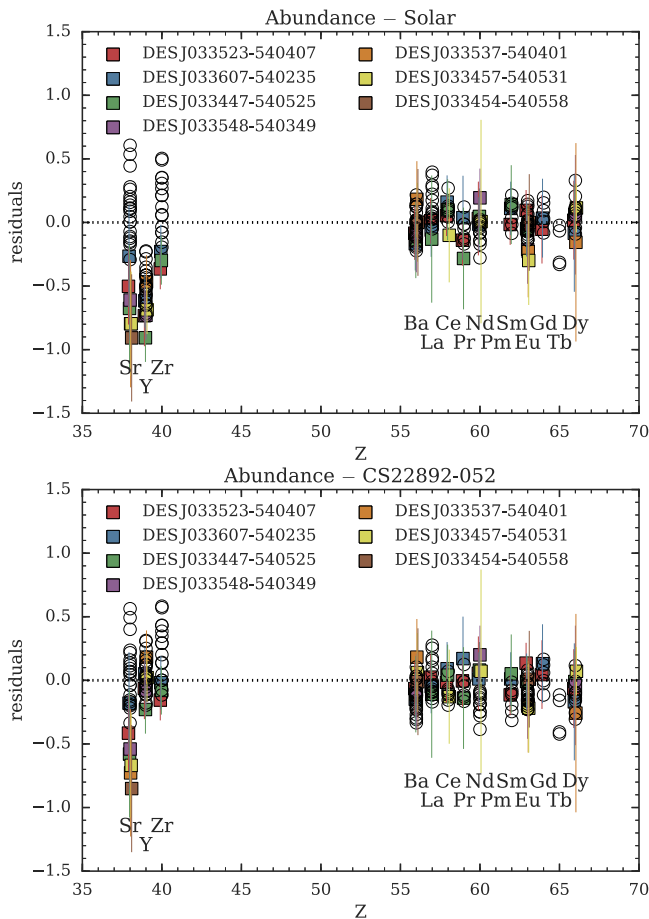
Figure 4. Abundance pattern residuals after subtracting the *r*-process pattern. The scaling is chosen according to Equation (1). Top panel: residual from the solar *r*-process pattern (Burris et al. 2000). Bottom panel: residual from CS22892-052 (Sneden et al. 2003). Colored squares with error bars indicate Ret II stars. Black circles indicate *r*-II stars (Aoki et al. 2007b, 2010; Frebel 2010; Roederer et al. 2014c; Li et al. 2015).

minimize the square of the residual of the heavy *r*-process elements weighted by the inverse abundance error (i.e., the χ^2):

$$\min_{\epsilon_{\text{offset}}} \sum_{X} \left(\frac{\log \epsilon (X_{\text{star}}) - (\log \epsilon (X_\odot) + \epsilon_{\text{offset}})}{\sigma_X} \right)^2, \qquad (1)$$

where X is all available abundance measurements of heavy *r*-process elements (Ba through Dy) for a given star, $\log \epsilon (X_{\text{star}})$ is the abundance of that element in the star, σ_X is the standard deviation of that abundance (Table 3), and $\log \epsilon (X_\odot)$ is the solar *r*-process residual (Burris et al. 2000).

The top panel of Figure 4 shows the resulting residuals. For comparison, we also plot residuals for *r*-II halo stars in black circles. For the elements above Ba, the residuals have a relatively small scatter (standard deviation of 0.07–0.18 dex). However, the Sr, Y, and Zr abundances lie systematically below the zero-residual line by an average of 0.4–0.7 dex (depending on the star). This is also true of some *r*-II stars (as found in, e.g., Travaglio et al. 2004; Montes et al. 2007).

The abundance pattern of the *r*-II star CS22892−052 is often regarded as a representative *r*-process pattern for both heavy and light *r*-process elements (e.g., Travaglio et al. 2004). In the bottom panel of Figure 4, we replace $\log \epsilon (X_\odot)$ in Equation (1) with $\log \epsilon (X)$ from CS22892−052 (Sneden et al. 2003). The Y

abundances in Ret II match those of CS22892−052 and the other *r*-II halo stars. The Zr abundances are consistent with that of CS22892−052 but lie at the low end of the abundance range for *r*-II halo stars. The Sr abundances appear to be lower than those of CS22892−052 and the halo stars. The Sr abundance is derived from two saturated lines with abundances that are sensitive to microturbulence, and the 4077 Å line is blended with La and Dy. However, the Sr abundances derived from spectra with higher signal-to-noise ratios in Roederer et al. (2016b) also display a slightly lower Sr abundance relative to the CS22892−052 pattern when the pattern is scaled according to Equation (1). Additionally, if one assumes [Sr/Fe] is the same in these seven *r*-process stars, the average Sr residual is significantly lower than that of CS22892−052. We also note that a variety of sources contribute to the *r*-II star abundances in Figure 4, and they may use slightly different analysis methods, resulting in systematic abundance differences. A completely homogeneous analysis is likely needed to quantify the true extent of the abundance scatter of Sr, Y, and Zr in these stars (the largest current homogeneous analysis can be found in Roederer et al. 2014a). Based on the current data, the behavior of the neutron-capture element residuals is certainly interesting, and we discuss possible implications in Section 4.1.

The majority of other UFDs have very low abundances or limits on their neutron-capture abundances ([Ba/H] $\lesssim -4$). An exception is a star in CVn II, which has an extremely high Sr abundance and a low Ba limit ([Sr/Fe] $= 1.32$, [Ba/Fe] < -1.28 François et al. 2016). The constraint [Sr/Ba] > 2.60 is one of the most extreme ratios known (compare to HD122563 with [Sr/Ba] $= 0.78$, Honda et al. 2007). As the abundances for the CVn II star were derived from intermediate-resolution spectra ($R \sim 8000$ in the bluest arm where the neutron-capture element lines are found), abundance analysis of a high-resolution spectrum of this star is needed to confirm its nature. At least one other star analyzed with high-resolution spectroscopy also has [Sr/Ba] > 2 (Jacobson et al. 2015).

The neutron-capture element abundances in the larger dwarf spheroidal galaxies have also been previously examined (e.g., Shetrone et al. 2001, 2003; Aoki et al. 2007b; Cohen & Huang 2009, 2010; Tsujimoto et al. 2015). We discuss some of these in Section 5.2. The *r*-process content of several globular clusters has also been investigated (see, e.g., Roederer et al. 2016a) for a thorough discussion). Of particular note is the globular cluster M15, which displays a large neutron-capture element dispersion (e.g., Otsuki et al. 2006).

3.6. Comparison to Literature Measurements

Our high-resolution [Fe/H] measurements are somewhat lower than previous medium-resolution measurements (Koposov et al. 2015b; Simon et al. 2015; Walker et al. 2015). Eight stars in our sample have [Fe/H] measurements in Simon et al. (2015) and Koposov et al. (2015b), from which we find a mean metallicity difference of -0.17 dex from Simon et al. (2015) and -0.38 dex from Koposov et al. (2015b). The large offset relative to Koposov et al. (2015b) may be due to significant differences in the stellar parameters, as on average they derive T_{eff} and $\log g$ values 300 K and 0.49 dex above our measurements, respectively, and thus find most of the stars at the base of the red giant branch. From the seven stars in common with Walker et al. (2015), we find a mean metallicity offset of -0.20 dex.

The brightest four stars in our sample were also observed by Roederer et al. (2016b). The abundance measurements are largely consistent once differences in stellar parameters are considered (within 0.1–0.2 dex). A notable exception is the heavy neutron-capture element abundances in DES J033523 −540407, where Roederer et al. (2016b) determine abundances that are 0.3−0.4 dex higher on average, a discrepancy not explainable by a difference in stellar parameters. Adopting the same line list reduces this offset by ∼50%. The remaining difference likely results from noise in the spectra, differences in continuum placement, and the difference between synthesis and equivalent widths. Roederer et al. (2016b) have better signal-to-noise per pixel for this star, although with a smaller wavelength coverage, resulting in fewer lines per element. We identify DES J033607−540235 as a CEMP star, while Roederer et al. (2016b) do not. This star is on the cusp of the CEMP definition, and our carbon abundances differ by less than 0.1 dex. We find that this is explained by differences in the employed carbon line lists.

4. NUCLEAR ASTROPHYSICS AND THE r-PROCESS SITE

We first discuss whether the universal r-process pattern extends to the lighter r-process elements in the context of Ret II (Section 4.1). We then elaborate on the discussion in Ji et al. (2016a) about the r-process site (Section 4.2). Finally, we consider possible evidence from UFDs for two r-process sites (Section 4.3).

There are three abundance peaks associated with the r-process, corresponding to different magic neutron numbers (e.g., Sneden et al. 2008, and references within). In this section, we use the term "light r-process elements" to refer to elements in the first peak, such as Sr, Y, and Zr. We use the term "heavy r-process elements" to refer to elements in the second and third peaks, including the elements above Ba.

4.1. Universality of Light r-process Elements

It is remarkable that the relative abundances of neutron-capture elements in r-process halo stars so closely match the scaled solar r-process residual for the heavy r-process elements. However, this universal r-process pattern may not extend to light r-process elements. As seen in the top panel of Figure 4, many r-II stars have significantly lower light r-process element abundances compared to the scaled solar r-process pattern (when scaled to the heavy r-process elements). Furthermore, within the r-II halo star sample, the scatter in abundance of the light r-process elements is large compared to the scatter in the heavy r-process elements (∼0.1 versus ∼0.2 dex, Sneden et al. 2008; also found within our r-II sample, see Figure 4).

If the r-process pattern is universal for both light and heavy r-process elements, then the stars in Ret II should most clearly showcase this pattern. Any contamination by other sources of neutron-capture elements is likely no more than the measured abundance of Sr in the non-r-process star DES J033531 −540148 ([Sr/Fe] = −1.73, Roederer et al. 2016b), or the Sr and Ba abundance level found in any of the other UFDs. Both of these levels are several orders of magnitude lower than what is observed in the r-process-enhanced Ret II stars. Furthermore, it appears extremely likely that the light r-process elements in the r-process-enhanced Ret II stars are predominantly produced

at the same astrophysical site as the heavy r-process elements, as it is unlikely that two different prolific neutron-capture events occurred in the same galaxy while not occurring in most UFDs (see Ji et al. 2016a).

It has sometimes been assumed that other metal-poor r-II stars (particularly CS22892−052) display a universal r-process pattern for both light and heavy r-process elements. Subtracting this pattern from the scaled solar r-process residual yields evidence for the existence of an additional process that produces mostly light r-process elements, but little or none of the heavy r-process elements (Travaglio et al. 2004; Montes et al. 2007). Indeed, some metal-poor stars display neutron-capture element patterns dominated by light r-process elements (e.g., Honda et al. 2007). The overall similarity between the light and heavy r-process element abundances for Ret II stars and CS22892−052 may validate the use of that star as a template r-process abundance pattern for both light and heavy r-process elements, although the Ret II stars may have even lower light r-process element abundances (especially for Sr) and thus display a purer r-process pattern. We note that the majority of r-II stars appear to display light r-process element abundances that are slightly higher than CS22892−052 and the Ret II stars (see bottom panel of Figure 4). If the universal r-process pattern extends to the light r-process elements, then those r-II stars are displaying a combination of the universal r-process pattern and an additional light r-process element source.

An alternative is that the observed scatter in relative light r-process elements reflects a true variation in the underlying nucleosynthetic sources. Theoretical calculations have found that the light and heavy r-process elements tend to be produced in the distinct ejecta components of a single astrophysical site (e.g., Wanajo et al. 2014; Just et al. 2015; Nishimura et al. 2015; Radice et al. 2016), providing some motivation for why universality might not be expected. If this is the case, the stars in Ret II would have to be enriched by a source producing a particularly low amount of light r-process elements.

4.2. Site of the r-process

Although the general features of the r-process have been understood since Burbidge et al. (1957), the exact site of the r-process is still not known. Core-collapse supernovae were proposed as a possible site early on, but the exact mechanism was unclear. Promising mechanisms include a high-entropy neutrino wind from the proto-neutron-star (e.g., Meyer et al. 1992; Woosley & Hoffman 1992; Kratz et al. 2007), or jets of material from highly magnetized and rotating proto-neutron stars (e.g., Cameron 2003; Winteler et al. 2012; Nishimura et al. 2015). The primary alternative to supernovae is neutron star mergers, where tidal unbinding of neutron-rich material results in copious r-process element production (e.g., Lattimer & Schramm 1976; Goriely et al. 2011; Wanajo et al. 2014; Just et al. 2015). Interest in this scenario has recently increased because the decaying r-process elements may produce "kilonova" afterglows, an optical counterpart to short gamma-ray burst or gravitational wave triggers (e.g., Metzger et al. 2010).

Multiple lines of evidence have provided somewhat conflicting conclusions about which of these sites is most important in the early universe. Chemical evolution models of abundance trends in metal-poor halo stars have tended to favor supernovae, as the delay times for neutron star mergers are

thought to be too large to affect low-metallicity stars (e.g., Argast et al. 2004; Matteucci et al. 2014). However, neutrino wind models have had difficulty producing the heavy *r*-process elements (e.g., Arcones et al. 2007; Arcones & Montes 2011; Wanajo 2013), while neutron star mergers seem to easily produce robust heavy *r*-process element patterns (Goriely et al. 2011; Wanajo et al. 2014; Lippuner & Roberts 2015). In addition, there is evidence for kilonova afterglows following short gamma-ray bursts (Berger et al. 2013; Tanvir et al. 2013; Yang et al. 2015), and radioactive isotopes in the interstellar medium suggest that *r*-process production is rare and prolific in the Milky Way today (Hotokezaka et al. 2015; Wallner et al. 2015). At this time, neutron star mergers thus appear to be the most likely *r*-process site in the local universe.

These different lines of evidence can be reconciled in galactic chemical evolution models with a combination of both supernovae and neutron star mergers (e.g., Cescutti et al. 2015; Wehmeyer et al. 2015). Alternatively, a pure neutron star merger enrichment scenario appears viable in models that include hierarchical galaxy formation and inefficient star formation (Tsujimoto & Shigeyama 2014a, 2014b; Ishimaru et al. 2015; Shen et al. 2015; van de Voort et al. 2015), models with binary formation in dense stellar environments that increases the rate of mergers (Ramirez-Ruiz et al. 2015), or chemical evolution models using lower supernova iron yields (Vangioni et al. 2016).

Ret II adds to these lines of evidence by providing context for the origin of its metal-poor stars. Ji et al. (2016a) were able to estimate the rate and yield of the *r*-process event by using information on the galactic environment in Ret II, as well as the population of UFDs as tracers of early star formation. They estimated the rate by considering the total number of super-novae across 10 UFDs, finding that one *r*-process event occurred in ∼2000 supernovae. There are significant uncertainties associated with this estimate, most notably the possibility of a different initial mass function in UFDs (Geha et al. 2013, although also see Fraser et al. 2015). Ji et al. (2016a) also estimated the yield of the *r*-process event ($M_{\rm Eu} \sim 10^{-4.5\pm1}\,M_\odot$) by considering typical metal dilution gas masses in UFDs in conjunction with the observed [Eu/H] ratios. More sophisticated hydrodynamic simulations of these dilution masses in the aftermath of a supernova explosion or neutron star merger (e.g., Bland-Hawthorn et al. 2015; Ritter et al. 2015; Montes et al. 2016) may be able to further constrain the dilution mass and thus the yield of the event.

The discovery of so many *r*-process stars in Ret II prompts us to revisit the origin of *r*-II halo stars. Many chemical evolution models of *r*-process elements consider just the formation of the Milky Way and assume that metal-poor halo stars (including *r*-II stars) trace the early history of the Galaxy (e.g., Argast et al. 2004; Matteucci et al. 2014; Wehmeyer et al. 2015). However, the halo also contains many stars stripped from accreted galaxies of varying masses (e.g., Zolotov et al. 2009; Pillepich et al. 2014). The stripped stars trace a different chemical evolution history compared to the full Milky Way, as their original host galaxies have lower star formation efficiencies and overall gas masses (e.g., Tsujimoto & Shigeyama 2014a, 2014b; Ishimaru et al. 2015; Rani et al. 2016). We suggest that *r*-II halo stars may predominantly be composed of stars stripped from *r*-process UFDs like Ret II. The characteristic UFD dark matter halo mass of $\sim 10^{7-8}\,M_\odot$ (e.g., Bland-Hawthorn et al. 2015; Ji et al. 2015) may be
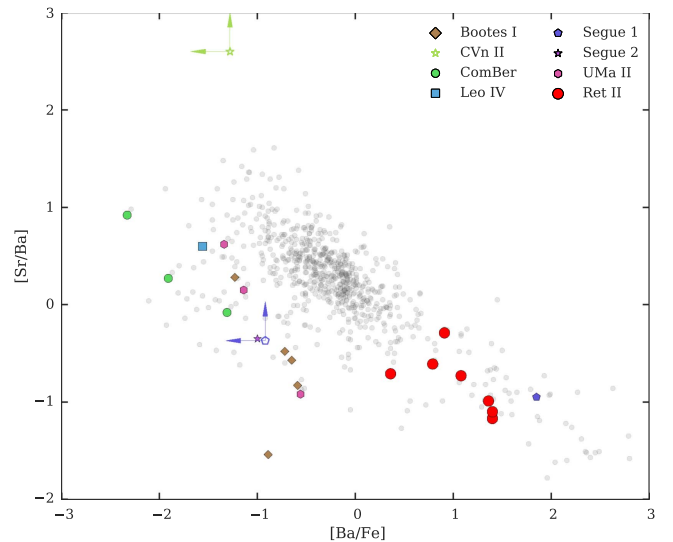
Figure 5. [Sr/Ba] vs. [Ba/Fe] for halo stars and UFD stars. Halo stars are only plotted if both Sr and Ba are measured. With the exception of Ret II and possibly CVn II, the UFD stars lie on a different [Sr/Ba] track than the majority of halo stars. The star in Segue 1 with high [Ba/Fe] has experienced binary mass transfer (Frebel et al. 2014).

connected to the observation that *r*-II stars are found almost exclusively at [Fe/H] ∼ −3 (e.g., Barklem et al. 2005). In addition, if neutron star mergers are the source of the *r*-process elements in *r*-II stars, then *r*-II stars must form in environments with low star-formation efficiencies in order to accomodate the neutron star merger delay time (Dominik et al. 2012).

4.3. Two r-process Sites?

The neutron-capture element content of stars in UFDs other than Ret II and CVn II is small but nonzero (Roederer 2013). It is not currently known what mechanism produces these small amounts of neutron-capture elements. One possibility is an *r*-process operating in supernovae (e.g., Frebel et al. 2010, 2014; Arcones & Montes 2011; Lee et al. 2013; Wanajo 2013). Alternatively, the *s*-process in metal-free spinstars could be responsible (e.g., Frischknecht et al. 2012). Unfortunately, in all UFD stars other than Ret II, Sr and Ba are the only neutron-capture elements detectable, and they have been measured in only a few stars. It is difficult to identify the source of this Sr and Ba without abundances of other neutron-capture elements.

However, these two elements illustrate an important difference between halo stars and UFD stars. In Figure 5 we plot [Sr/Ba] and [Ba/Fe] for these two samples. Halo stars are only plotted if they have both Sr and Ba measurements, and UFD stars are only plotted if they have at least one measurement of Sr or Ba. The halo stars show a trend that [Sr/Ba] decreases as [Ba/Fe] increases. The UFD stars (other than Ret II and CVn II) also seem to obey a trend in Sr and Ba, but it is offset from the main halo trend. This suggests that whatever produced the neutron-capture elements in most UFDs is not responsible for the majority of neutron-capture element production. However, the Ret II stars are consistent with the overall halo star trend.

One way to interpret Figure 5 is that two *r*-process sites exist. One site is common but inefficient, responsible for the small amount of neutron-capture elements found in most UFDs. This site is presumably ordinary core-collapse

supernovae (e.g., Arcones & Montes 2011; Wanajo 2013), which would explain the apparent ubiquity of neutron-capture elements in metal-poor stars (Roederer et al. 2010a; Roederer 2013). Variations in the electron fraction or entropy of supernova ejecta (e.g., Farouqi et al. 2010; Roederer et al. 2010a) or strongly mass-dependent supernova yields (e.g., Lee et al. 2013) might explain the varying [Sr/Ba] ratios from this site, although it is still unclear whether heavy r-process elements can be synthesized in supernovae (e.g., Wanajo 2013). The other r-process site is rare and prolific, such as a neutron star merger or jet supernova. This site is responsible for the bulk of r-process material in Ret II. The existence of multiple r-process sites has been suggested several times before (e.g., Wasserburg et al. 1996; Qian & Wasserburg 2007, 2008; Tsujimoto & Shigeyama 2014b; Cescutti et al. 2015; Wehmeyer et al. 2015). However, the offset in Figure 5 between UFD stars and most halo stars suggests that the bulk of neutron-capture elements are not synthesized by the common but inefficient r-process site. As the Ret II stars follow the halo star trend, this may indicate that rare and prolific events are responsible for the majority of r-process material in halo stars.

5. EARLY STAR AND GALAXY FORMATION

5.1. Star Formation Timescale and Inhomogenous Metal Mixing in Ret II

Core-collapse supernovae produce enhanced [α/Fe] ratios (∼0.4), which are reflected in the abundances of metal-poor stars (e.g., Tinsley 1979). The simplest chemical evolution signature is the [α/Fe] ratio as a function of [Fe/H]. This ratio typically decreases with metallicity, signifying the onset of iron production in SNe Ia (e.g., Venn et al. 2004; Kirby et al. 2011a; Vargas et al. 2013). If the ratio remains elevated, then the galaxy stopped forming stars prior to enrichment by SNe Ia, and it is a possible first galaxy candidate (Frebel & Bromm 2012; Frebel et al. 2014). Our Ret II stars include two relatively high-metallicity stars ([Fe/H] ∼ −2), DES J033548−540349 and DES J033457−540531 that can be used to test whether there is a decline.

Interestingly, these two stars appear to have a fundamentally different character from each other. DES J033548−540349 has several lower metal ratios in the lighter elements (Mg, Si, Sc), and its neutron-capture element enhancement is less strong than in the other Ret II r-process stars observed. This suggests that it formed after some SN Ia enrichment. In contrast, DES J033457−540531 shows similar metal ratios to the lower-metallicity r-process stars (i.e., both [α/Fe] and [Sr, Ba, Eu/Fe] enhanced), but at a metallicity almost one dex higher than the other stars. Our observations of DES J033457−540531 have low signal-to-noise, and strong conclusions based on this star await better data. Supposing that our measurements are confirmed by future observations, one explanation would be that DES J033457−540531 formed from extremely inhomogeneously mixed gas: the overall metallicity varied by one order of magnitude, but the metal ratios stayed the same. Unlike α-elements, which have a degeneracy between inhomogenous metal mixing and multiple bursts of star formation (e.g., Webster et al. 2016), copious r-process enrichment is unlikely to happen more than once in the system (Ji et al. 2016a). If inhomogeneous mixing is required to explain this star, it would imply that iron was mixed in a similar fashion to the r-process elements, and

possibly suggest that iron was produced concurrently with these elements.

Evidence for inhomogeneous metal mixing is also found in other Ret II stars. The three lower metallicity r-process stars all have [Fe/H] ∼ −3 but widely varying metal ratios [X/Fe]. For example, Roederer et al. (2016b) have already pointed out the very large discrepancy in carbon abundances for DES J033523−540407 and DES J033607−540235. The Si and Mn abundances also appear to vary substantially.

The two most metal-poor stars in the system (DES J033531−540148 and DES J033556−540316) are also the two stars with very low neutron-capture element abundances [Ba/Fe] < 0. The most straightforward interpretation is that these stars formed in Ret II prior to the r-process enrichment event. However, the clear presence of inhomogeneous metal mixing suggests that we cannot rule out the possibility that they formed later from a pocket of low-metallicity gas without r-process enrichment. There is also a possibility that these stars were once members of a smaller galaxy that merged into Ret II (e.g., Tolstoy et al. 2004). Merger trees from cosmological zoom-in simulations suggest that this is unlikely if Ret II is hosted by a dark matter halo of peak mass ≲$10^{8.5} M_\odot$, but the chance of this occurring increases with larger halo masses (B. F. Griffen et al. 2016, in preparation).

5.2. r-process in dSphs

The r-process content of stars in larger dSph galaxies has already been considered. The Draco and Ursa Minor dSphs stand out in particular. Draco has one star with high [Eu/Fe], and its general abundance trend shows a flat [Eu/H] starting from [Fe/H] ≳ −2.3 (Shetrone et al. 2001; Cohen & Huang 2009; Tsujimoto et al. 2015). Draco also has one star with exceptionally low neutron-capture abundances, with [Ba/Fe] < −2.6 (Fulbright et al. 2004). In contrast, Ursa Minor has several stars with elevated [Eu/Fe] ∼ 0.5 (Cohen & Huang 2010), including one star (COS 82) with [Fe/H] ∼ −1.5 that has [Eu/Fe] ≳ 1 (Shetrone et al. 2001; Sadakane et al. 2004; Aoki et al. 2007b). The Draco stars appear to show signatures of s-process enrichment, while Ursa Minor appears to be uncontaminated by the s-process (Cohen & Huang 2009, 2010).

Despite their similar present-day luminosities (Irwin & Hatzidimitriou 1995; Martin et al. 2008), Draco and Ursa Minor likely have different gas accretion histories. Kirby et al. (2011b) studied the metallicity distribution functions (MDF) in these and other dSphs. They found that the observed MDF in most dSphs requires significant gas accretion, which is well motivated from typical mass-accretion histories of dark matter halos in ΛCDM cosmology (Wechsler et al. 2002; Kirby et al. 2011a). If gas accretion is unimportant in Draco, the flat [Eu/H] feature would favor rare and prolific Eu-enrichment events (Tsujimoto et al. 2015). However, if gas accretion is as important as the MDF suggests, then the flat [Eu/H] feature would instead suggest that continual r-process enrichment, perhaps from normal core-collapse supernovae, is actually the dominant source of Eu in this system (Ji et al. 2016a). In contrast to most dSphs, the Ursa Minor MDF does not appear to require such gas accretion (Kirby et al. 2011b).

5.3. Signatures of the First Stars

The small number of enriching stellar generations and the simple environment suggests that UFDs are one of the best places to find chemical signatures from the first generation of stars (Frebel & Bromm 2012; Karlsson et al. 2013; Ji et al. 2015). One of the most promising signatures is the increasing fraction of carbon-enhanced metal-poor (CEMP) stars at low metallicity, which may be associated with the initial mass function of Pop III stars (e.g., Norris et al. 2013; Cooke & Madau 2014).

Three of the r-process enhanced stars in Ret II are CEMP stars. These stars all have [Fe/H] ~ -3, resulting in a cumulative CEMP fraction of $\sim 40\%$ which is similar to the halo CEMP fraction for [Fe/H] $\geqslant -3$ (Placco et al. 2014). However, at least one of the two stars in Ret II with [Fe/H] < -3 (i.e., the two without r-process enhancement) is *not* a CEMP star. We can only provide a carbon upper limit for the most metal-poor star in our sample (DES J033556−540316). If the gas in Ret II was well mixed and stars formed sequentially with metallicity (as opposed to concurrent formation out of inhomogeneously mixed gas), then it seems that copious carbon enrichment occurred *after* the formation of these first two metal-poor stars.

Another tantalizing possibility is that the r-process event may be somehow related to Pop III stars. A Pop III neutron star binary would maximize the time delay between adjacent generations of star formation, since Pop III stars form in smaller dark matter halos, allowing supernova feedback to be more effective (e.g., Whalen et al. 2008). Furthermore, the initial mass function of Pop III stars is thought to be top-heavy (e.g., Greif et al. 2011), which might result in more massive binaries compared to a standard initial mass function. Simulations suggest Pop III stars have a binary fraction of $\sim 35\%$ (Stacy & Bromm 2013). Metal-poor stars are also more likely to have the rapid rotation rate required for jet supernovae (see discussion in Winteler et al. 2012), and this may extend to metal-free stars. r-process nucleosynthesis in Pop III stars clearly deserves further examination.

6. CONCLUSION

We present the complete chemical abundances for nine stars in Reticulum II spanning the full metallicity distribution of the galaxy, from $-3.5 < $ [Fe/H] < -2. Seven of the stars have high neutron-capture element abundances consistent with the universal r-process pattern (Ji et al. 2016a). The other two stars are the lowest metallicity stars in our sample ([Fe/H] < -3; Figure 3). The relative abundance of light neutron-capture elements (Sr, Y, Zr) in the r-process-enhanced stars is significantly lower than that of the solar r-process pattern. These abundances are mostly consistent with those of the r-II star CS22892−052, but lower than those of most other r-II stars (Figure 4). In our current spectra, heavier r-process elements in the third r-process peak (e.g., Pb), as well as the actinides Th and U, cannot be detected. All other elements (up to the iron peak) have abundances generally consistent with stars in the halo and in other UFDs, although there is internal scatter in several metal ratios (Figure 2).

The galactic context for Ret II stars provides a unique opportunity to identify the source of r-process elements and constrain the formation history of the galaxy. Chemical evolution models of Ret II constructed for this purpose will likely need to account for inhomogeneous metal mixing, which is indicated by the internal abundance scatter for several elements (Figure 2). Ret II also shows that galactic chemical evolution models of r-process elements in halo stars must account for hierarchical galaxy formation. While Ret II was enriched by a rare and prolific event, the presence of small amounts of neutron-capture elements in other UFDs may suggest two different r-process sites (Figure 5).

The r-process stars in Ret II likely provide the cleanest r-process pattern found to date across all three r-process peaks. In principle, this could provide the best available r-process pattern for nucleosynthesis calculations. However, the stars in this galaxy are far away and faint, precluding detailed abundance studies at the level currently possible in halo stars. More detailed abundance studies of this galaxy may need to await high-resolution spectroscopy from the next generation of 30-meter class telescopes.

REFERENCES

Aoki, W., Beers, T. C., Christlieb, N., et al. 2007a, ApJ, 655, 492
Aoki, W., Beers, T. C., Honda, S., & Carollo, D. 2010, ApJL, 723, L201
Aoki, W., Honda, S., Sadakane, K., & Arimoto, N. 2007b, PASJ, 59, L15
Arcones, A., Janka, H.-T., & Scheck, L. 2007, A&A, 467, 1227
Arcones, A., & Montes, F. 2011, ApJ, 731, 5
Argast, D., Samland, M., Thielemann, F.-K., & Qian, Y.-Z. 2004, A&A, 416, 997
Asplund, M., Grevesse, N., Sauval, A. J., & Scott, P. 2009, ARA&A, 47, 481
Astropy Collaboration, Robitaille, T. P., Tollerud, E. J., et al. 2013, A&A, 558, A33
Barklem, P. S., Christlieb, N., Beers, T. C., et al. 2005, A&A, 439, 129
Bechtol, K., Drlica-Wagner, A., Balbinot, E., et al. 2015, ApJ, 807, 50
Berger, E., Fong, W., & Chornock, R. 2013, ApJL, 774, L23
Bernstein, R., Shectman, S. A., Gunnels, S. M., Mochnacki, S., & Athey, A. E. 2003, Proc. SPIE, 4841, 1694
Bland-Hawthorn, J., Sutherland, R., & Webster, D. 2015, ApJ, 807, 154
Bohlin, R. C., Jenkins, E. B., Spitzer, L., Jr., et al. 1983, ApJS, 51, 277
Brown, T. M., Tumlinson, J., Geha, M., et al. 2014, ApJ, 796, 91
Burbidge, E. M., Burbidge, G. R., Fowler, W. A., & Hoyle, F. 1957, RvMP, 29, 547
Burris, D. L., Pilachowski, C. A., Armandroff, T. E., et al. 2000, ApJ, 544, 302
Cameron, A. G. W. 2003, ApJ, 587, 327
Casey, A. R. 2014, arXiv:1405.5968
Casey, A. R., & Schlaufman, K. C. 2015, ApJ, 809, 110
Castelli, F., & Kurucz, R. L. 2004, arXiv:astro-ph/0405087
Cescutti, G., Romano, D., Matteucci, F., Chiappini, C., & Hirschi, R. 2015, A&A, 577, A139
Christlieb, N., Beers, T. C., Barklem, P. S., et al. 2004, A&A, 428, 1027
Cohen, J. G., & Huang, W. 2009, ApJ, 701, 1053
Cohen, J. G., & Huang, W. 2010, ApJ, 719, 931

Cooke, R. J., & Madau, P. 2014, ApJ, 791, 116
Den Hartog, E. A., Lawler, J. E., Sneden, C., & Cowan, J. J. 2003, ApJS, 148, 543
Dominik, M., Belczynski, K., Fryer, C., et al. 2012, ApJ, 759, 52
Drlica-Wagner, A., Albert, A., Bechtol, K., et al. 2015, ApJL, 809, L4
Farouqi, K., Kratz, K.-L., Pfeiffer, B., et al. 2010, ApJ, 712, 1359
François, P., Monaco, L., Bonifacio, P., et al. 2016, A&A, 588, A7
Fraser, M., Casey, A. R., Gilmore, G., Heger, A., & Chan, C. 2015, arXiv:1511.03428
Frebel, A. 2010, AN, 331, 474
Frebel, A., & Bromm, V. 2012, ApJ, 759, 115
Frebel, A., Casey, A. R., Jacobson, H. R., & Yu, Q. 2013, ApJ, 769, 57
Frebel, A., Christlieb, N., Norris, J. E., et al. 2007, ApJL, 660, L117
Frebel, A., Christlieb, N., Norris, J. E., Aoki, W., & Asplund, M. 2006, ApJL, 638, L17
Frebel, A., Norris, J. E., Gilmore, G., & Wyse, R. F. G. 2016, ApJ, 826, 110
Frebel, A., Simon, J. D., Geha, M., & Willman, B. 2010, ApJ, 708, 560
Frebel, A., Simon, J. D., & Kirby, E. N. 2014, ApJ, 786, 74
Frischknecht, U., Hirschi, R., & Thielemann, F.-K. 2012, A&A, 538, L2
Fulbright, J. P., Rich, R. M., & Castro, S. 2004, ApJ, 612, 447
Geha, M., Brown, T. M., Tumlinson, J., et al. 2013, ApJ, 771, 29
Gilmore, G., Norris, J. E., Monaco, L., et al. 2013, ApJ, 763, 61
Goriely, S., Bauswein, A., & Janka, H.-T. 2011, ApJL, 738, L32
Greif, T. H., Springel, V., White, S. D. M., et al. 2011, ApJ, 737, 75
Hayek, W., Wiesendahl, U., Christlieb, N., et al. 2009, A&A, 504, 511
Hill, V., Plez, B., Cayrel, R., et al. 2002, A&A, 387, 560
Honda, S., Aoki, W., Ishimaru, Y., & Wanajo, S. 2007, ApJ, 666, 1189
Honda, S., Aoki, W., Kajino, T., et al. 2004, ApJ, 607, 474
Hotokezaka, K., Piran, T., & Paul, M. 2015, NatPh, 11, 1042
Howes, L. M., Casey, A. R., & Asplund, M., et al. 2015, Natur, 527, 484
Hunter, J. D. 2007, CSE, 9, 90
Irwin, M., & Hatzidimitriou, D. 1995, MNRAS, 277, 1354
Ishigaki, M. N., Aoki, W., Arimoto, N., & Okamoto, S. 2014, A&A, 562, A146
Ishimaru, Y., Wanajo, S., & Prantzos, N. 2015, ApJL, 804, L35
Ivans, I. I., Simmerer, J., Sneden, C., et al. 2006, ApJ, 645, 613
Jacobson, H. R., Keller, S., Frebel, A., et al. 2015, ApJ, 807, 171
Ji, A. P., Frebel, A., & Bromm, V. 2015, MNRAS, 454, 659
Ji, A. P., Frebel, A., Chiti, A., & Simon, J. D. 2016a, Natur, 531, 610
Ji, A. P., Frebel, A., Simon, J. D., & Geha, M. 2016b, ApJ, 817, 41
Jones, E., Oliphant, T., Peterson, P., et al. 2001, SciPy: Open Source Scientific Tools for Python
Just, O., Bauswein, A., Pulpillo, R. A., Goriely, S., & Janka, H.-T. 2015, MNRAS, 448, 541
Karlsson, T., Bromm, V., & Bland-Hawthorn, J. 2013, RvMP, 85, 809
Keeping, E. S. 1962, Introduction to Statistical Inference (Princeton, NJ: Van Nostrand)
Kelson, D. D. 2003, PASP, 115, 688
Kim, Y.-C., Demarque, P., Yi, S. K., & Alexander, D. R. 2002, ApJS, 143, 499
Kirby, E. N., Cohen, J. G. Guhathakurta, P., et al. 2013, ApJ, 779, 102
Kirby, E. N., Cohen, J. G., Smith, G. H., et al. 2011a, ApJ, 727, 79
Kirby, E. N., Lanfranchi, G. A., Simon, J. D., Cohen, J. G., & Guhathakurta, P. 2011b, ApJ, 727, 78
Kirby, E. N., Simon, J. D., Geha, M., Guhathakurta, P., & Frebel, A. 2008, ApJL, 685, L43
Koch, A., Feltzing, S., Adén, D., & Matteucci, F. 2013, A&A, 554, A5
Koch, A., McWilliam, A., Grebel, E. K., Zucker, D. B., & Belokurov, V. 2008, ApJL, 688, L13
Koposov, S. E., Belokurov, V., Torrealba, G., & Evans, N. W. 2015a, ApJ, 805, 130
Koposov, S. E., Casey, A. R., Belokurov, V., et al. 2015b, ApJ, 811, 62
Kratz, K.-L., Farouqi, K., Pfeiffer, B., et al. 2007, ApJ, 662, 39
Lai, D. K., Bolte, M., Johnson, J. A., et al. 2008, ApJ, 681, 1524
Lattimer, J. M., & Schramm, D. N. 1976, ApJ, 210, 549
Lawler, J. E., Den Hartog, E. A., Sneden, C., & Cowan, J. J. 2006, ApJS, 162, 227
Lawler, J. E., Sneden, C., Cowan, J. J., Ivans, I. I., & Den Hartog, E. A. 2009, ApJS, 182, 51
Lee, D. M., Johnston, K. V., Tumlinson, J., Sen, B., & Simon, J. D. 2013, ApJ, 774, 103
Li, H.-N., Aoki, W., Honda, S., et al. 2015, RAA, 15, 1264
Lind, K., Asplund, M., Barklem, P. S., & Belyaev, A. K. 2011, A&A, 528, A103
Lippuner, J., & Roberts, L. F. 2015, ApJ, 815, 82
Martin, N. F., de Jong, J. T. A., & Rix, H.-W. 2008, ApJ, 684, 1075
Masseron, T., Plez, B., Van Eck, S., et al. 2014, A&A, 571, A47

Matteucci, F., Romano, D., Arcones, A., Korobkin, O., & Rosswog, S. 2014, MNRAS, 438, 2177
McConnachie, A. W. 2012, AJ, 144, 4
Metzger, B. D., Martínez-Pinedo, G., Darbha, S., et al. 2010, MNRAS, 406, 2650
Meyer, B. S., Mathews, G. J., Howard, W. M., Woosley, S. E., & Hoffman, R. D. 1992, ApJ, 399, 656
Montes, F., Beers, T. C., Cowan, J., et al. 2007, ApJ, 671, 1685
Montes, G., Ramirez-Ruiz, E., Naiman, J., Shen, S., & Lee, W. H. 2016, arXiv:1601.05808
Nishimura, N., Takiwaki, T., & Thielemann, F.-K. 2015, ApJ, 810, 109
Nomoto, K., Kobayashi, C., & Tominaga, N. 2013, ARA&A, 51, 457
Norris, J. E., Wyse, R. F. G., Gilmore, G., et al. 2010a, ApJ, 723, 1632
Norris, J. E., Yong, D., Bessell, M. S., et al. 2013, ApJ, 762, 28
Norris, J. E., Yong, D., Gilmore, G., & Wyse, R. F. G. 2010b, ApJ, 711, 350
Otsuki, K., Honda, S., Aoki, W., Kajino, T., & Mathews, G. J. 2006, ApJL, 641, L117
Pillepich, A., Vogelsberger, M., Deason, A., et al. 2014, MNRAS, 444, 237
Placco, V. M., Frebel, A., Beers, T. C., & Stancliffe, R. J. 2014, ApJ, 797, 21
Preston, G. W., Sneden, C., Thompson, I. B., Shectman, S. A., & Burley, G. S. 2006, AJ, 132, 85
Qian, Y.-Z., & Wasserburg, G. J. 2007, PhR, 442, 237
Qian, Y.-Z., & Wasserburg, G. J. 2008, ApJ, 687, 272
Radice, D., Galeazzi, F., Lippuner, J., et al. 2016, MNRAS, arXiv:1601.02426
Ramirez-Ruiz, E., Trenti, M., MacLeod, M., et al. 2015, ApJL, 802, L22
Rani, A. S., Sivarani, T., Beers, T. C., et al. 2016, MNRAS, 458, 2648
Ritter, J. S., Sluder, A., Safranek-Shrader, C., Milosavljević, M., & Bromm, V. 2015, MNRAS, 451, 1190
Roederer, I. U. 2013, AJ, 145, 26
Roederer, I. U., Cowan, J. J., Karakas, A. I., et al. 2010a, ApJ, 724, 975
Roederer, I. U., Cowan, J. J., Preston, G. W., et al. 2014a, MNRAS, 445, 2970
Roederer, I. U., & Kirby, E. N. 2014, MNRAS, 440, 2665
Roederer, I. U., Mateo, M., Bailey, J. I., et al. 2016a, MNRAS, 455, 2417
Roederer, I. U., Mateo, M., Bailey, J. I., III, et al. 2016b, AJ, 151, 82
Roederer, I. U., Preston, G. W., Thompson, I. B., et al. 2014b, AJ, 147, 136
Roederer, I. U., Preston, G. W., Thompson, I. B., Shectman, S. A., & Sneden, C. 2014c, ApJ, 784, 158
Roederer, I. U., Sneden, C., Thompson, I. B., Preston, G. W., & Shectman, S. A. 2010b, ApJ, 711, 573
Sadakane, K., Arimoto, N., Ikuta, C., et al. 2004, PASJ, 56, 1041
Shen, S., Cooke, R. J., Ramirez-Ruiz, E., et al. 2015, ApJ, 807, 115
Shetrone, M., Venn, K. A., Tolstoy, E., et al. 2003, AJ, 125, 684
Shetrone, M. D., Côté, P., & Sargent, W. L. W. 2001, ApJ, 548, 592
Simon, J. D., Drlica-Wagner, A., Li, T. S., et al. 2015, ApJ, 808, 95
Simon, J. D., Frebel, A., McWilliam, A., Kirby, E. N., & Thompson, I. B. 2010, ApJ, 716, 446
Simon, J. D., & Geha, M. 2007, ApJ, 670, 313
Simon, J. D., Geha, M., Minor, Q. E., et al. 2011, ApJ, 733, 46
Sneden, C., Cowan, J. J., & Gallino, R. 2008, ARA&A, 46, 241
Sneden, C., Cowan, J. J., Lawler, J. E., et al. 2003, ApJ, 591, 936
Sneden, C., Lawler, J. E., Cowan, J. J., Ivans, I. I., & Den Hartog, E. A. 2009, ApJS, 182, 80
Sneden, C. A. 1973, PhD thesis, Univ. Texas
Sobeck, J. S., Kraft, R. P., Sneden, C., et al. 2011, AJ, 141, 175
Stacy, A., & Bromm, V. 2013, MNRAS, 433, 1094
Strigari, L. E., Bullock, J. S., Kaplinghat, M., et al. 2008, Natur, 454, 1096
Tanvir, N. R., Levan, A. J., Fruchter, A. S., et al. 2013, Natur, 500, 547
Tinsley, B. M. 1979, ApJ, 229, 1046
Tolstoy, E., Irwin, M. J., Helmi, A., et al. 2004, ApJL, 617, L119
Travaglio, C., Gallino, R., Arnone, E., et al. 2004, ApJ, 601, 864
Tsujimoto, T., Ishigaki, M. N., Shigeyama, T., & Aoki, W. 2015, PASJ, 67, L3
Tsujimoto, T., & Shigeyama, T. 2014a, A&A, 565, L5
Tsujimoto, T., & Shigeyama, T. 2014b, ApJL, 795, L18
van de Voort, F., Quataert, E., Hopkins, P. F., Kereš, D., & Faucher-Giguère, C.-A. 2015, MNRAS, 447, 140
van der Walt, S., Colbert, S. C., & Varoquaux, G. 2011, CSE, 13, 22
Vangioni, E., Goriely, S., Daigne, F., François, P., & Belczynski, K. 2016, MNRAS, 455, 17
Vargas, L. C., Geha, M., Kirby, E. N., & Simon, J. D. 2013, ApJ, 767, 134
Venn, K. A., Irwin, M., Shetrone, M. D., et al. 2004, AJ, 128, 1177
Walker, M. G., Mateo, M., Olszewski, E. W., et al. 2015, ApJ, 808, 108
Wallner, A., Faestermann, T., Feige, J., et al. 2015, NatCo, 6, 5956
Wanajo, S. 2013, ApJL, 770, L22
Wanajo, S., Sekiguchi, Y., Nishimura, N., et al. 2014, ApJL, 789, L39
Waskom, M., Botvinnik, O., drewokane, et al. 2016, seaborn, v0.7.0, Zenodo, zenodo.45133

Wasserburg, G. J., Busso, M., & Gallino, R. 1996, ApJL, 466, L109

Webster, D., Frebel, A., & Bland-Hawthorn, J. 2016, ApJ, 818, 80

Wechsler, R. H., Bullock, J. S., Primack, J. R., Kravtsov, A. V., & Dekel, A. 2002, ApJ, 568, 52

Wehmeyer, B., Pignatari, M., & Thielemann, F.-K. 2015, MNRAS, 452, 1970

Weisz, D. R., Dolphin, A. E., Skillman, E. D., et al. 2014, ApJ, 789, 148

Westin, J., Sneden, C., Gustafsson, B., & Cowan, J. J. 2000, ApJ, 530, 783

Whalen, D., van Veelen, B., O'Shea, B. W., & Norman, M. L. 2008, ApJ, 682, 49

Winteler, C., Käppeli, R., Perego, A., et al. 2012, ApJL, 750, L22

Wise, J. H., Demchenko, V. G., Halicek, M. T., et al. 2014, MNRAS, 442, 2560

Woosley, S. E., & Hoffman, R. D. 1992, ApJ, 395, 202

Yang, B., Jin, Z.-P., Li, X., et al. 2015, NatCo, 6, 7323

Zolotov, A., Willman, B., Brooks, A. M., et al. 2009, ApJ, 702, 1058